American Mineralogist, Volume 72, pages 201–208, 1987

Barian tomichite, $Ba_{0.5}(As_2)_{0.5}Ti_2(V,Fe)_5O_{13}(OH)$, its crystal structure and relationship to derbylite and tomichite

Ian E. Grey, Ian C. Madsen
CSIRO Division of Mineral Chemistry, P.O. Box 124, Port Melbourne, Victoria 3207, Australia
Donald C. Harris
Geological Survey of Canada, 601 Booth Street, Ottawa Ontario K1A 0E8, Canada

Abstract

Barian tomichite, ideally $Ba_{0.5}(As_2)_{0.5}Ti_2(V,Fe)_5O_{13}(OH)$, is monoclinic, space group $A2/m$, $Z = 2$, with $a = 7.105(4)$, $b = 14.217(4)$, $c = 5.043(2)$ Å and $\beta = 104.97(7)°$. Its structure has been determined and refined to $R = 0.054$ for 1128 unique reflections, collected on a Siemens AED diffractometer using Mo$K\alpha$ radiation. The structure is closely related to that of derbylite, $SbTi_3Fe_4O_{13}(OH)$, and is based on a closest-packed anion framework with a stacking sequence ($hhc\cdots$). Small cations are ordered into 14 of the 30 octahedral sites per unit cell, forming α-PbO_2- and V_3O_5-type chains of edge-shared octahedra along [001]. In the cubic-stacked anion layers, two anions per unit cell are missing, forming cuboctahedral cavities that are occupied by Ba and by As_2^{3+} pairs (in pyramidal coordination with their lone-electron pairs directed toward the missing anion position). The refinement was carried out for the average structure, in which Ba and As_2 statistically occupy the same cavity. Long-exposure precession photographs showed diffuse superlattice reflections due to an ordering of Ba and As_2 in successive sites along [001]. Results of a refinement of the related mineral tomichite, $AsTi_3(V,Fe)_4O_{13}(OH)$ are also reported.

Introduction

An investigation of V-bearing oxide minerals from the "green leader" gold lodes at Kalgoorlie, Western Australia (Nickel, 1977), led to the characterization of the new mineral tomichite, $AsTi_3(V,Fe)_4O_{13}(OH)$ (Nickel and Grey, 1979). Single-crystal and powder X-ray diffraction data showed that the tomichite is isostructural with derbylite, $SbTi_3Fe_4O_{13}(OH)$, with As replacing Sb and V replacing Fe. A structure refinement for derbylite (Moore and Araki, 1976) in space group $P2_1/m$ showed that the structure is based on a closest packing of anions with stacking sequence (*chh*) and with the Sb and its electron lone pair forming part of the anion framework. The remaining cations are ordered in octahedral sites, forming edge-shared octahedral columns and chains.

A recently discovered gold deposit in Hemlo, Canada, bears some resemblance to the Kalgoorlie "green leader" deposit, particularly in relation to the presence of V-bearing micas, garnets, rutiles, and other oxides. During a study of drill-core samples from the Hemlo deposit, one of us (D.C.H.) identified an oxide mineral with V, Ti, As, and Sb, whose X-ray powder pattern is similar to those of tomichite and derbylite. However, in contrast to these two minerals, which contain only small cations, the Hemlo material contains a significant amount of the large cation Ba (3.6–7.5 wt% BaO from different drill-core samples). Single-crystal XRD studies on the mineral show that it has unit-cell parameters similar to those of tomichite, i.e., $a = 7.10$, $b = 14.22$, $c = 5.04$ Å, $\beta = 104.9°$, but a different space group, $A2/m$. In addition, long-exposure precession photographs revealed the presence of weak, diffuse superlattice reflections, with an incommensurate periodicity along **a***. We report here a description of the mineral and the determination and refinement of its average structure in space group $A2/m$, as well as a structure refinement for tomichite.

Occurrence and composition

Barian tomichite is present in drill core from the newly discovered Hemlo gold deposit, Ontario, Canada. The deposit is located near the northeast shore of Lake Superior, 300 km east of Thunder Bay or 35 km east of Marathon, adjacent to the Trans-Canada Highway (17). The strata-bound deposit, which is of Archean age, occurs at the contact between felsic metavolcanic and metasedimentary rocks. The mineralization is substantially enriched in Mo, Sb, As, Hg, Tl, V, and Ba. The deposit contains a diverse assemblage of minerals with the major ore minerals consisting of pyrite, molybdenite, stibnite, zinkenite, tetrahedrite, sphalerite, realgar, cinnabar, and aktashite with minor to trace amounts of 36 other metallic minerals. The gangue minerals are principally quartz, barite, sericite, vanadian muscovite, rutile, and barian microcline. Barian tomichite is a minor constituent, and it only occurs in the central barite-rich part of the deposit, embedded in quartz and microcline feldspar as anhedral to subhedral tabular grains ranging from 0.1 to 3 mm in maximum dimensions. It is present in several drill holes

0003–004X/87/0102–0201$02.00

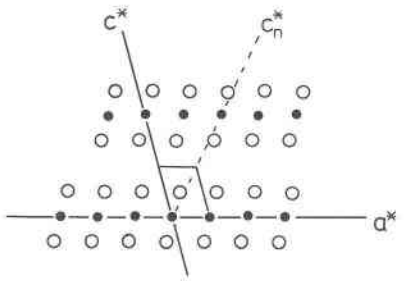

Fig. 1. Schematic representation of ($h0l$) reciprocal lattice section for barian tomichite. Subcell reflections are indicated by filled circles and superlattice reflections by open circles. Displacement of superlattice reflections along **a*** is slightly exaggerated to emphasize the orientation anomaly.

Table 1. Microprobe analyses for barian tomichite phases

Drill core sample	W70-754.4 (11 analyses)	GG20-884.0 (4 analyses)	GG14W-879.55 (6 analyses)
TiO_2	26.39	34.65	27.23
V_2O_3	38.82	23.10	34.78
BaO	6.31	3.55	7.58
Fe_2O_3	9.96	19.29	13.14
Al_2O_3	0.93	1.07	0.98
Sb_2O_3	2.00	3.31	0.81
As_2O_3	12.81	12.52	13.27

Formulae normalized to 13 oxygens + OH and 7 cations in the M site.

W70-754.4 $(Ba_{0.29}As_{0.91}Sb_{0.10})(Ti_{2.33}V_{3.66}Fe^{2+}_{0.86}Al_{0.13})O_{13}(OH)$

GG20-884.0 $(Ba_{0.16}As_{0.88}Sb_{0.16})(Ti_{3.02}V_{2.15}Fe^{2+}_{0.46}Fe^{3+}_{1.22}Al_{0.15})O_{13}(OH)$

GG14W-879.55 $(Ba_{0.35}As_{0.95}Sb_{0.04})(Ti_{2.41}V_{3.29}Fe^{2+}_{0.08}Fe^{3+}_{1.09}Al_{0.13})O_{13}(OH)$

and is commonly associated with pyrite, molybdenite, stibnite, native arsenic, sphalerite, zinkenite, aktashite, tetrahedrite, and vanadian muscovite. In hand specimens, barian tomichite is black in color with a metallic to submetallic luster, conchoidal fracture, and a black streak. In polished section, the reflection color is gray in air with weak to moderate anisotropism between crossed nicols.

Average microprobe analyses for samples from three different drill cores are given in Table 1. A large number of analyses have been carried out on samples taken from different depths, and from different areas at the same depth, and a detailed analysis of the results will be published elsewhere. They may be summarized in terms of the following interelement correlations: (1) strong negative correlation between Ba and Sb, (2) strong negative correlation between V and (Fe + Ti), (3) moderate positive correlation between V and Ba, (4) moderate positive correlations between Fe and Ti and between Ba and As, and (5) moderate negative correlations between As and Sb and between Fe and V.

The crystal used for the structure analysis was selected from the sample having the highest Ba content, listed as GG14W-879.55 in Table 1. The formula, normalized to 13 oxygens + OH [as for derbylite, Moore and Araki (1976)] is

$$(Ba_{0.35}As_{0.95}Sb_{0.04})(Ti_{2.41}V^{3+}_{3.29}Fe^{2+}_{0.08}Fe^{3+}_{1.09}Al_{0.13})O_{13}(OH),$$

where the Fe^{2+}/Fe^{3+} ratio has been adjusted to give charge balance. Because of the close compositional relationship to tomichite (Nickel and Grey, 1979) we refer to the mineral as a barian tomichite.

Single-crystal studies

Precession studies

Crystals excavated from polished section GG14W-879.55 were first examined by the precession method. They were confirmed to have monoclinic symmetry, with cell parameters similar to those reported for tomichite (Nickel and Grey, 1979) and derbylite (Moore and Araki, 1976), namely, $a \simeq 7.1$, $b \simeq 14.2$, $c \simeq 5.0$ Å and $\beta \simeq 104.9°$. However, in contrast to these latter two minerals, the diffraction patterns for the barian tomichite display the general extinction, (hkl), $k + l = 2n$ corresponding to an A-centered cell, with possible space groups Am, $A2$ or $A2/m$. Furthermore, long-exposure precession photographs revealed the presence of weak, diffuse superlattice reflections corresponding to a superstructure with apparent doubling of the a and c parameters. Careful measurement of the superlattice reflection positions shows that they are slightly displaced along **a*** from the positions corresponding to $[n(h/2), n(l/2)]$, n odd. This is illustrated in the schematic representation of the ($h0l$) reciprocal lattice section in Figure 1. If a new subcell c_n^* direction is chosen, corresponding to $\beta^* = 64.5°$ (shown by the dashed line in Fig. 1), then the superlattice reflections occur in pairs about each subcell reflection and exhibit an orientation anomaly of about 7° relative to c_n^*. In the following structure analysis and refinement, we consider only the sharp subcell reflections that correspond to diffraction from the average structure.

Experimental details

For the data collection, an orthogonal crystal measuring 0.130 × 0.214 × 0.108 mm was mounted along **b*** on a Siemens AED 3-circle diffractometer. Cell dimensions, refined using the 2θ values for 12 centered high-angle ($36° < 2\theta < 71°$) reflections are $a = 7.105(4)$, $b = 14.217(4)$, $c = 5.043(2)$ Å, $\beta = 104.97(7)°$, Mo$K\alpha_1$, $\lambda = 0.7093$. A total of 2251 intensities was collected to a maximum 2θ value of 70°, using the θ–2θ scan mode with scan width $(2.4° + \Delta\theta)$, where $\Delta\theta = \Delta\lambda/(2d \cos\theta)$ allows for α_1/α_2 separation, and a scan speed of $0.033°/s^{-1}$. The backgrounds were counted for 40 s on each side of each reflection. A standard reflection, measured every 2 h, showed less than 1.5% variation in intensity. After correcting for absorption ($\mu_l = 116.2$ cm^{-1}; transmission factors between 0.14 and 0.330), reduction and averaging of the intensities yielded 1128 unique reflections with agreement between equivalent reflections, $R_{int} = 0.029$.

Scattering factors for neutral atoms, and anomalous dispersion coefficients were taken from *International Tables for X-ray Crystallography* (1974). All computing was performed with SHELX-76 system of programs (Sheldrick, 1976).

Structure solution and refinement

The similarity between the cell parameters and powder-diffraction pattern of the barian tomichite and those of derbylite suggested a close relationship between the two structures. It was found that the octahedral framework of derbylite could be described in $A2/m$ after introducing an origin shift of (½,¼,¾). Refinement was begun using the transformed derbylite coordinates for the octahedral cations M (V, Ti and Fe), and As. The Ba atom and oxygen atoms were located in subsequent difference

Table 2. Barian tomichite—Atomic coordinates and thermal vibration parameters

Atom	x	y	z	U_{11}	U_{22}	U_{33}	U_{23}	U_{13}	U_{12}
M(1)	0	0	0	0.0086(7)	0.0078(7)	0.0087(7)	0	0.0016(5)	0
M(2)	0	0.6172(1)	0	0.0079(3)	0.0141(5)	0.0102(5)	0	0.0034(4)	0
M(3)	0.3171(1)	0.1916(1)	0.1185(2)	0.0060(3)	0.0074(3)	0.0062(3)	−0.0007(2)	0.0025(2)	−0.0018(2)
Ba*	0.5	0.5	0	0.0102(7)	0.0084(6)	0.0095(7)	0	−0.0028(5)	0
As*	0.5807(2)	0	0.2396(3)	0.0032(5)	0.0047(5)	0.0099(7)	0	0.0013(4)	0
O(1)	0.1593(5)	0.0983(3)	0.2329(8)	0.008(1)	0.008(1)	0.009(1)	0.000(1)	0.003(1)	−0.001(1)
O(2)	0.1741(5)	0.2985(3)	0.2275(7)	0.008(1)	0.010(1)	0.006(1)	0.001(1)	0.000(1)	0.003(1)
O(3)	0.5	0.2859(4)	0	0.006(2)	0.008(2)	0.006(2)	0	0.002(2)	0
O(4)	0.5	0.0947(4)	0	0.015(2)	0.008(2)	0.016(2)	0	0.002(2)	0
O(5)	0.1488(8)	0	0.7175(11)	0.011(2)	0.009(2)	0.010(2)	0	0.004(2)	0

* Site occupancies of Ba and As are 0.35 and 0.47, respectively.

Fourier maps. The scattering curve for V was used for the individual M sites. With the Ba occupancy determined from the microprobe-analysis data, refinement of all positional and anisotropic thermal parameters converged to an R value of 0.056. The largest feature in the final difference Fourier map was a peak of height ~2 e/Å^3 near As, at (0.58, 0, 0.36). Bond-length calculations indicated that this was due to substitution of minor Sb for As. With inclusion of Sb at the above position, refinement of all parameters converged at $R = 0.054$ (unit weights) for all 1128 unique reflections. The final refinement involved 64 independent parameters and the largest shift/error was 0.09.

Final atomic position and thermal vibration parameters are given in Table 2. Selected bond lengths and angles are given in Table 3. Tables 4 and 5 listing the observed and calculated structure factors have been deposited.[1]

[1] To obtain copies of Tables 4 and 5 order Document AM-87-327 from the Business Office, Mineralogical Society of America, 1625 I Street, N.W., Suite 414, Washington, D.C. 20006. Please remit $5.00 in advance for the microfiche.

Description of structure

Barian tomichite, like derbylite (Moore and Araki, 1976), has a structure based on a closest-packing of anions with a stacking sequence ($hhc\cdots$). Small cations (Ti^{4+}, V^{3+}, Fe^{3+}) are ordered in 14 of the 30 octahedral sites per unit cell. In the (100) cubic-stacked anion layers, two anions per unit cell are vacant, creating cuboctahedral cavities centered at the special positions 2d (½,½,0 and ½,0,½). In derbylite, these cavities are occupied by Sb^{3+} and its lone pair of electrons (the Sb is displaced from the cavity center), whereas in the barian tomichite, partial occupancy by Ba occurs (centrally located at ½,½,0, ½,0,½). The occupancy is completed with As^{3+} and its lone electron pair (together with minor Sb).

The structure is made up by stacking (100) layers of octahedra of two types, illustrated in Figure 2. Between pairs of h-stacked anion layers, small cations occupy 60%

Table 3. Barian tomichite—Polyhedral bond lengths (Å) and angles (°)

	M(1) octahedron		
4	M(1)–O(1)	1.982(4)	
2	–O(5)	1.980(6)	
			O-M-O
2	O(1)–O(1)	2.795(9)	89.6(2)
2	–O(1)′	2.813(7)	90.4(2)
4	–O(5)	2.662(6)	84.4(2)
4	–O(5)′	2.935(7)	95.6(2)
	M(3) octahedron		
	M(3)–O(1)	1.919(4)	
	–O(2)	1.976(3)	
	–O(2)′	1.983(4)	
	–O(3)	2.053(1)	
	–O(3)′	2.059(4)	
	–O(4)	2.083(4)	
	O(1)–O(2)	2.849(6)	93.7(2)
	–O(2)′	2.966(6)	99.1(2)
	–O(3)	2.951(5)	95.9(2)
	–O(4)	2.950(4)	94.9(2)
	O(2)–O(2)′	2.874(4)	93.1(1)
	–O(3)	2.656(4)	82.3(1)
	–O(3)′	2.656(4)	82.3(1)
	–O(3)″	2.841(4)	89.3(2)
	–O(4)	2.814(5)	87.7(1)
	O(3)–O(3)′	2.720(4)	82.8(1)
	–O(4)	3.040(5)	94.6(1)
	–O(4)′	2.718(8)	82.0(2)
	M(2) octahedron		
2	M(2)–O(2)	1.885(4)	
2	–O(1)	1.988(4)	
2	–O(5)	2.121(3)	
			O-M-O
2	O(1)–O(2)	2.837(6)	94.1(2)
2	–O(2)′	2.872(6)	95.7(2)
2	O(1)–O(5)	2.662(6)	80.7(2)
2	–O(5)′	2.833(7)	87.1(2)
	O(2)–O(2)	2.910(6)	101.0(2)
2	–O(5)	2.870(4)	91.3(2)
	O(5)–O(5)	2.63(1)	76.5(2)
	Ba cuboctahedron		
4	Ba–O(1)	2.820(4)	
2	–O(3)	3.045(5)	
4	–O(4)	2.858(3)	
2	–O(5)	2.972(6)	
2	O(1)–O(1)′	2.795(9)	59.4(2)
4	–O(3)	2.951(5)	60.3(2)
4	–O(4)	2.950(4)	62.6(1)
4	–O(5)	2.833(7)	58.5(2)
4	O(3)–O(4)	3.040(5)	61.9(2)
2	O(4)–O(4)′	2.69(1)	56.2(2)
4	–O(5)	2.871(5)	59.0(2)
	As pyramid		
2	As–O(4)	1.802(4)	
	–O(5)	1.878(6)	
	O(4)–O(4)′	2.69(1)	96.7(2)
2	–O(5)	2.871(5)	102.5(1)

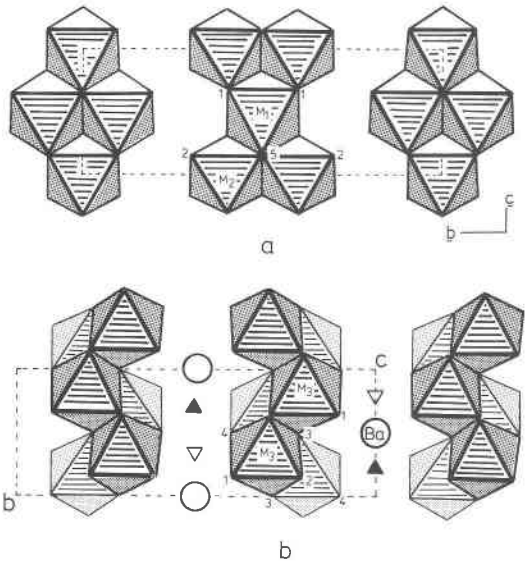

Fig. 2. Octahedral layers in barian tomichite. (a) V_3O_5-type layers, formed between pairs of *h*-stacked anion layers. (b) Layers comprising α-PbO_2-type chains of edge-shared octahedra, formed between pairs of *h*- and *c*-stacked anion layers. The fusing together of pairs of layers of this type by octahedral edge-sharing is shown. Oxygens are labeled according to Table 2. Arsenic at $x = 0.42$ and 0.58 is shown by open and filled triangles.

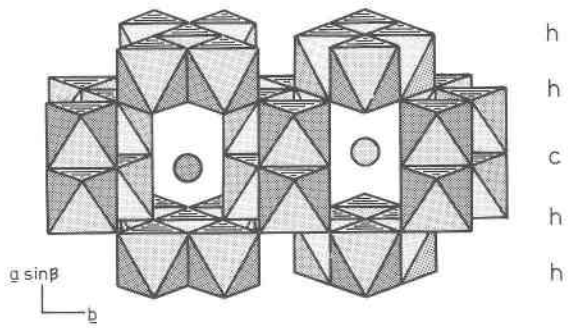

Fig. 3. Polyhedral representation of the structure of barian tomichite, viewed along [001], depicting tunnels bound by the V_3O_5 columns, above and below, and by the fused α-PbO_2-type double chains at the sides. The cuboctahedral cavities in these tunnels contain Ba and (As,Sb). Labeling of *h*- and *c*-stacked anion layers is shown.

of the octahedral interstices to form a layer of V_3O_5-type structure (Åsbrink et al., 1959). As shown in Figure 2a, this structure comprises [001] columns of edge-shared octahedra, alternately one- and two-octahedra wide. Between pairs of *c*- and *h*-stacked anion layers, 40% of the octahedral sites are occupied, forming α-PbO_2-type (Zaslavskiy and Tolkachev, 1952) zigzag chains of edge-shared octahedra along [001]. The chains are in mirror-relation across (010) planes at $y = 0$ and $y = ½$. These layers occur in pairs, *h*-M-*c*-M-*h*, across the *c*-stacked anion layer that contains the Ba atom. The α-PbO_2 chains in adjacent layers are linked together by edge-sharing, as shown in Figure 2b.

A polyhedral representation of the structure of barian tomichite, viewed approximately along [001] in Figure 3, portrays it as a tunnel structure, where the tunnels have α-PbO_2-type double chains as walls and V_3O_5 columns at top and bottom, the different units being linked by corner-sharing. The tunnel alternately constricts and expands along [001] as the width of the V_3O_5 columns changes from one to two octahedra. The latter gives rise to a cuboctahedral cavity, occupied by Ba and (As,Sb). These cations cannot occupy the cavity at the same time, and ordering occurs, giving rise to the observed superstructure (Fig. 1).

Polyhedral bond lengths and angles are given in Table 3. Using Zachariasen's (1978) empirical bond length–bond strength parameters, the valence sums at the different cation sites have been calculated, giving an estimate of site occupation, M(1) = 0.55Ti + 0.45(V,Fe), M(2) = 0.45Ti + 0.55(V,Fe), M(3) = 0.24Ti + 0.76(V,Fe), where the V and Fe are trivalent, except for a minor component of Fe^{2+} in M(3).

The average As–O bond length of 1.826 Å is somewhat longer than values reported in the literature for pyramidal As^{3+}, e.g., in reinerite, $Zn_3(AsO_3)_2$, the average As–O bond length is 1.774 Å (Ghose et al., 1977) and reflects the partial substitution of Sb for As. The Ba atom is in the center of a cubic-stacked anion sequence and so has cuboctahedral coordination to oxygen. The mean Ba–O distance is 2.895 Å, which is well within the range of mean Ba–O distances of 2.84 to 2.97 Å reported for barium titanates (Tillmans et al., 1985).

Structure-composition relationships

Ordering of Ba and (As,Sb)

The structure refinement confirms that the barian tomichite unit cell comprises 14 small cations and 28 anions, forming an octahedral framework enclosing two cuboctahedral cavities, in which reside the Ba and (As,Sb) cations. The position of the Ba and (As,Sb) cations within a cuboctahedron is shown in Figure 4. Evidently Ba and (As,Sb) cannot occupy the same cavity because the Ba–As separation is only 1.56 Å. In the related structure of derbylite, only one trivalent ion (Sb^{3+}) occupies each cavity, whereas in barian tomichite, multiple occupancy by the smaller As^{3+} must occur to explain the observed Σ(Ba + As,Sb) > 1 (i.e., 1.34). A reasonable model for occupancy of the tunnels, consistent with the analytical data, is 0.35Ba + 0.35(As_2) + 0.29(As,Sb), involving occupancy of some of the cuboctahedra by pairs of AsO_3 pyramids, having their lone pairs of electrons both directed toward the missing anion site. Here, As_2 refers to two As atoms occupying the same cavity, as shown in Figure 4, with As–As = 3.12 Å, rather than to covalently bonded pairs, as in $FeAs_2$, where As–As = 2.49 Å (Kjekshus et al., 1974). Along the tunnels, ordering of Ba and (As_2) in successive cuboctahedral cavities is expected to occur and is the most likely explanation for the observed superlattice (Fig. 1). The third tunnel component, (As,Sb), singly occupies the

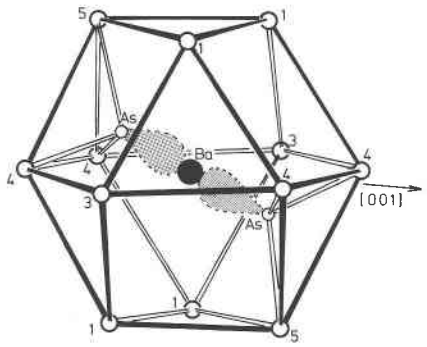

Fig. 4. Location of Ba and As atoms in the cuboctahedral cavity. Oxygen atoms are labeled according to Table 2. In the ordered structure, successive cuboctahedral cavities along [001] contain alternately Ba and $(As)_2$ pairs. Arsenic lone-pair electron orbitals are shown schematically.

cuboctahedral cavity as in derbylite. The Sb will be concentrated in these regions. Intergrowth of regions of Ba–(As_2) with regions of (As,Sb) explains the observed negative correlations between Sb and (Ba,As). The derbylite-like regions must be very small and uncorrelated, as no violation of the *A*-centering was detected. It is possible that the intergrowths occur in an ordered way at the unit-cell level and may be the origin of the orientation anomalies shown in Figure 1.

Valence-sum calculations

The calculation of the valence sums at the different cation sites, given in the previous section, gives $\Sigma M^{n+} = 23.2$. When combined with Ba^{2+} and (As^{3+},Sb^{3+}), the total positive charge per asymmetric unit formula is 26.9. With 14 anions per asymmetric unit, this requires 13 oxygens + OH for charge balance, as reported for derbylite (Moore and Araki, 1976).

We attempted to verify the formulation of barian tomichite as an oxyhydroxide by infrared spectroscopy (IR) and thermogravimetric analysis (TGA). The IR evidence was inconclusive; only a very weak broad band at 3400 cm^{-1} was observed that could be attributed to OH. TGA runs showed a gradual weight loss of the correct magnitude (1–1.5 wt%) in the temperature range 400–600°C. The weight loss was difficult to measure accurately as it overlapped with a large weight-loss step due to volatilization of As.

Although direct evidence for hydroxyls was not convincing, valence-sum calculations for the cavity anions are consistent with an oxyhydroxide model. In Table 6, the effect of the different cavity components on the valence sums of the coordinated oxygens is given. For the derbylite-like regions, the four-fold site O(5) splits into two two-fold sites, with only one of these coordinated to (As,Sb). Consistent with the model proposed by Moore and Araki (1976), one of these sites is severely undersaturated, with a valence sum of 1.32, and is considered to be occupied by OH^-. The corresponding formula is $(As,Sb)M_7O_{13}(OH)$.

Table 6. Effect of cuboctahedral-cavity component on valence sums to coordinated oxygens

Cavity component	Anion	Coordinated cation	M–O	Valence sum	
Ba	O(4)	2 × M(3)	2.083		
		Ba	2.858	1.04	(OH)
	O(5)	2 × M(2)	2.121		
		M(1)	1.980		
		Ba	2.972	1.49	(H-bond O)
(As_2)	O(4)	2 × M(3)	2.083		
		2 × As	1.802	2.22	(O)
	O(5)	2 × M(2)	2.121		
		M(1)	1.980		
		As	1.878	1.91	(O)
(As,Sb)	O(4)	2 × M(3)	2.083		
		As	1.802	1.52	(H-bond O)
	O(5)′	2 × M(2)	2.121		
	O(5)*	M(1)	1.980	1.32	(OH)
	O(5)″	2 × M(2)	2.121		
		M(1)	1.980		
		As	1.878	1.91	(O)

* O(5) splits into two two-fold sites in derbylite (Moore and Araki, 1976).

Where (As_2) pairs occupy the cavity, the valence sums at both anion sites O(4) and O(5) are close to 2, consistent with oxygen occupation of these sites. However, when Ba occupies the cuboctahedral cavity, the valence sum for O(4) is only 1.04, corresponding to OH occupancy of O(4). There is presumably H-bonding to O(5), with a valence sum of 1.49. As the atomic ratio of O(4) to Ba is 2, the corresponding composition for the ordered $Ba(As_2)$ regions is $Ba_{0.5}(As_2)_{0.5}M_7O_{13}(OH)$. This represents the ideal formula for endmember barian tomichite. The mineral studied here therefore represents a barian tomichite–dominant intergrowth structure with a minor component of the derbylite- (or tomichite-) type structure. The general formula is $[Ba_{0.5}(As_2)_{0.5}]_x(As,Sb)_{1-x}M_7O_{13}(OH)$, where $x = 0.7$ for the data crystal.

For derbylite, the ratio of M^{4+} to M^{3+} is 3:4, whereas for the barian tomichite endmember, the ratio is 2:5. This accords with the positive correlation between Ba and trivalent V. It is clear from the strong positive correlation between V and (Fe + Ti) that a substitution of the type

Table 7. Tomichite—Atomic coordinates and isotropic thermal vibration parameters

Atom	*x*	*y*	*z*	*B* (Å²)
M(1)	0.4965(10)	0.25	0.7453(14)	0.35(6)
M(2)	0.5017(6)	0.1289(2)	0.2484(10)	0.23(6)
M(3)	0.8171(5)	0.0606(3)	0.8736(8)	0.10(7)
M(4)	0.8195(5)	−0.0620(3)	0.3755(8)	0.15(7)
As	0.0789(5)	0.25	0.0125(8)	0.47(6)
O(1)	0.342(3)	0.25	0.033(4)	0.01(36)
O(2)	0.673(2)	−0.047(1)	−0.023(3)	0.50(28)
O(3)	0.654(2)	0.152(1)	−0.023(3)	0.19(26)
O(4)	0.003(3)	0.155(1)	0.756(4)	0.52(23)
O(5)	0.002(3)	0.034(1)	0.252(4)	0.45(23)
O(6)	0.677(2)	0.048(1)	0.483(3)	0.34(28)
O(7)	0.342(2)	0.152(1)	0.516(3)	0.43(29)
O(8)	0.647(3)	0.25	0.458(5)	0.38(43)

Table 8. Tomichite—Polyhedral bond lengths (Å) and angles (°)

	M(1) octahedron			M(2) octahedron		
1	M(1)–O(1)	2.02(2)		M(2)–O(6)	1.87(2)	
1	–O(8)	2.00(3)		–O(2)	1.85(2)	
2	–O(7)	1.95(2)		–O(3)	1.96(2)	
2	–O(3)	1.96(2)		–O(7)	1.99(2)	
			O–M–O	–O(8)	2.14(1)	
2	O(1)–O(3)	2.69(3)	84.9(7)	–O(1)	2.18(1)	
2	–O(7)	2.79(3)	95.3(7)			O–M–O
1	O(3)–O(3)	2.79(3)	90.5(9)	O(1)–O(2)	2.88(2)	90.5(6)
2	–O(7)	2.75(2)	89.1(6)	–O(3)	2.69(3)	80.7(8)
2	–O(8)	2.79(3)	95.4(7)	–O(7)	2.79(2)	83.6(8)
1	O(7)–O(7)′	2.78(3)	91.2(9)	–O(8)	2.62(3)	74.5(6)
2	–O(8)	2.65(3)	84.4(8)	O(2)–O(3)	2.81(2)	94.7(7)
				–O(6)	2.92(2)	103.6(7)
	As pyramid			–O(7)	2.85(2)	95.9(7)
2	As–O(4)	1.85(2)		O(3)–O(6)	2.89(2)	97.9(7)
1	–O(1)	1.84(2)		–O(8)	2.79(3)	85.7(9)
				O(6)–O(7)	2.84(2)	94.7(7)
2	O(1)–O(4)	2.79(2)	98.5(8)	–O(8)	2.87(2)	91.4(7)
	O(4)–O(4)′	2.71(3)	94.3(10)	O(7)–O(8)	2.65(3)	80.0(9)
	M(3) octahedron			M(4) octahedron		
	M(3)–O(3)	1.90 92)		M(4)–O(7)	1.89(2)	
	–O(6)	1.95(2)		–O(2)	2.00(2)	
	–O(2)	1.98(2)		–O(6)	2.01(2)	
	–O(4)	2.07(2)		–O(5)	2.00(2)	
	–O(5)	2.04(2)		–O(4)	2.05(2)	
	–O(5)′	2.07(2)		–O(5)′	2.08(2)	
	O(2)–O(3)	2.83(2)	93.6(7)	O(2)–O(4)	2.79(2)	87.2(7)
	–O(5)	2.64(2)	82.2(6)	–O(5)	2.64(2)	80.7(7)
	–O(6)	2.83(2)	91.7(7)	–O(6)	2.86(2)	91.1(7)
	O(3)–O(4)	2.97(3)	96.9(7)	–O(7)	2.96(2)	99.1(7)
	–O(5)	3.01(2)	99.6(7)	O(4)–O(5)	2.68(2)	80.9(7)
	–O(6)	2.91(2)	98.4(7)	–O(5)′	3.04(3)	97.6(7)
	O(4)–O(5)	3.01(3)	94.6(7)	–O(7)	2.96(3)	97.5(8)
	–O(5)′	2.68(2)	80.7(7)	O(5)–O(5)′	2.67(4)	81.5(8)
	–O(6)	2.80(2)	88.2(7)	–O(6)	2.59(2)	80.5(6)
	O(5)–O(5)	2.67(4)	81.8(8)	–O(6)′	2.84(3)	87.8(7)
	–O(6)	2.59(2)	80.4(7)	–O(7)	2.96(2)	98.8(7)
	O(2)–O(5)′	2.84(3)	88.8(7)	O(6)–O(7)	2.84(2)	93.7(7)

$2V^{3+} \rightleftharpoons Ti^{4+} + Fe^{2+}$ also occurs. This becomes important for small values of x (see Table 1, and compare with reported Fe^{2+}-bearing derbylite from Italy; Mellini et al., 1983).

It should also be mentioned that an alternative model for charge balance was considered, based on pairs of $(As_2O_7)^{4-}$ corner-shared tetrahedra containing As^{5+}, where the shared oxygen would occupy the center of the cuboctahedral cavity. However, it was not possible to locate the As atoms in positions that satisfied conditions both for reasonable As^{5+}–O mean bond lengths and also for the necessary lengthening of the corner-shared As–O bonds.

Relationship to tomichite

We have previously reported the discovery of a new titanate mineral, tomichite (Nickel and Grey, 1979), that is isostructural with derbylite but with As in place of Sb and with V as dominant trivalent element, having the ideal formula $AsTi_3V_4O_{13}(OH)$. Tomichite is chemically similar to the barian tomichite described here, but does not contain Ba, and the space group is primitive, $P2_1/m$. We have carried out a structure refinement of tomichite, using X-ray intensity data collected for a single crystal from the "green leader" gold deposit at Kalgoorlie, Western Australia. The chemical analysis and unit-cell parameters are reported by Nickel and Grey (1979).

The single crystal available for a structure refinement was very small, 0.03 × 0.04 × 0.07 mm, and the resulting intensity data set is inferior to that of barian tomichite with only 54% of reflections having $I > 3\sigma(I)$ (cf. 92% for barian tomichite). Using the derbylite coordinates (Moore and Araki, 1976) as a starting model, refinement of coordinates and isotropic thermal parameters converged at $R = 0.074$ for 537 observed reflections. The final parameters are listed in Table 7 and polyhedral bond lengths and angles are given in Table 8.

Using Zachariasen's (1978) empirical parameters, the bond lengths in Table 8 have been used to calculate valence sums at the cation sites, giving an estimate of the site occupancies. The results obtained are M(1) = 0.6Ti + 0.4(V,Fe), M(2) = 0.62Ti + 0.38(V,Fe), M(3) = 0.3Ti + 0.7(V,Fe), and M(4) = 0.27Ti + 0.73(V,Fe). In comparing these with the site occupancies for barian tomichite, note that the eight-fold site M(3) in the latter splits into two four-fold sites M(3) and M(4) in tomichite. These correspond to alternate cation sites along the α-PbO_2 chains. The unit-cell composition for the tomichite crystal studied here is $As_2Ti_6V_6Fe_2O_{26}(OH)_2$, compared with

Table 9. Calculated powder patterns for tomichite and barian tomichite

			Tomichite		Barian tomichite					Tomichite		Barian tomichite	
h	*k*	*l*	*d*	*I*	*d*	*I*	*h*	*k*	*l*	*d*	*I*	*d*	*I*
0	2	0	7.097	7	7.108	<1	1	0	2	2.111	4	2.129	7
1	0	0	6.857	2	6.864	1	1	6	$\bar{1}$	2.098	1		
1	1	0	6.174	8			3	3	$\bar{1}$	2.076	2	2.078	<1
1	2	0	4.931	23	4.938	6	3	3	0	2.058	1		
0	0	1	4.826	9			2	3	$\bar{2}$	2.046	1		
0	1	1	4.569	2	4.608	<1	1	2	2	2.024	20	2.040	16
0	1	$\bar{1}$	4.569	2	4.068	<1	0	4	2	1.995	2	2.009	<1
1	0	$\bar{1}$	4.539	7			0	4	$\bar{2}$	1.995	2	2.009	<1
1	1	$\bar{1}$	4.323	7	4.345	<1	1	6	1	1.967	1		
0	2	$\bar{1}$	3.991	6			3	0	$\bar{2}$	1.927	5	1.934	2
0	2	1	3.991	6			3	4	0	1.921	<1	1.924	1
1	3	0	3.894	2			2	4	$\bar{2}$	1.912	2	1.920	<1
1	2	$\bar{1}$	3.824	9			3	1	$\bar{2}$	1.910	1		
0	4	0	3.548	<1	3.554	6	2	5	1	1.878	6	1.885	3
1	0	1	3.538	3			0	7	1	1.869	<1	1.875	1
1	1	1	3.433	10	3.457	2	0	7	$\bar{1}$	1.869	<1	1.875	1
2	0	0	3.428	1	3.432	6	3	1	1	1.869	2	1.876	5
0	3	1	3.379	<1	3.397	2	3	2	$\bar{2}$	1.860	4	1.866	<1
0	3	$\bar{1}$	3.379	<1	3.397	2	1	7	$\bar{1}$	1.851	1	1.856	<1
2	1	0	3.332	5			1	4	2	1.814	<1	1.827	<1
1	3	$\bar{1}$	3.275	<1	3.287	3	3	5	$\bar{1}$	1.792	9	1.794	15
2	0	$\bar{1}$	3.216	1			3	5	0	1.780	1		
1	2	1	3.167	6			2	0	2	1.769	12	1.782	14
1	4	0	3.151	16	3.156	30	1	7	1	1.759	1	1.765	5
2	1	$\bar{1}$	3.136	<1	3.142	3	2	1	2	1.756	1		
2	2	0	3.087	38	3.091	64	4	1	$\bar{1}$	1.753	2	1.753	<1
2	2	$\bar{1}$	2.929	2			3	3	1	1.751	<1	1.757	1
0	4	1	2.859	2			1	8	0	1.718	5	1.720	2
0	4	$\bar{1}$	2.859	2			2	2	2	1.717	2	1.728	<1
1	3	1	2.834	86	2.848	100	2	7	$\bar{1}$	1.715	3	1.718	3
1	4	$\bar{1}$	2.795	4			4	0	0	1.714	<1	1.716	1
2	3	0	2.776	2			1	6	$\bar{2}$	1.714	13	1.722	5
2	3	$\bar{1}$	2.660	100	2.664	71	3	4	$\bar{2}$	1.694	<1	1.699	1
1	4	1	2.506	2			1	1	$\bar{3}$	1.654	<1	1.668	2
1	0	$\bar{2}$	2.487	27	2.507	16	3	6	0	1.644	5	1.646	2
2	1	1	2.467	2	2.479	7	2	6	$\bar{2}$	1.638	3	1.644	1
0	5	$\bar{1}$	2.447	8	2.456	6	2	1	$\bar{3}$	1.617	<1	1.629	2
0	5	1	2.447	8	2.456	6	4	0	$\bar{2}$	1.608	15	1.611	19
1	5	$\bar{1}$	2.407	3	2.413	8	2	8	0	1.576	14	1.578	17
0	6	0	2.366	10	2.369	12	3	5	1	1.570	26	1.575	33
1	2	$\bar{2}$	2.347	<1	2.364	1	3	7	$\bar{1}$	1.524	2	1.526	1
3	0	0	2.286	3	2.288	1	0	3	3	1.523	4	1.536	1
3	1	$\bar{1}$	2.280	2	2.282	<1	0	3	$\bar{3}$	1.523	4	1.536	1
2	0	$\bar{2}$	2.269	3	2.282	7	4	5	$\bar{1}$	1.500	15	1.501	11
3	1	0	2.256	2			4	1	1	1.498	2	1.494	3
2	1	$\bar{2}$	2.241	1			3	0	2	1.479	3	1.488	3
1	6	0	2.236	1	2.240	4	1	1	3	1.475	1	1.488	<1
1	5	1	2.214	12	2.223	20	3	3	$\bar{3}$	1.441	11	1.448	13
2	3	1	2.214	1	2.223	<1	1	5	$\bar{3}$	1.436	23	1.446	32
2	5	0	2.186	1			4	3	1	1.428	4	1.432	2
3	2	0	2.175	2	2.178	5	0	10	0	1.419	9	1.422	13
2	2	$\bar{2}$	2.162	3	2.173	11	1	3	3	1.415	1	1.427	4
2	5	$\bar{1}$	2.128	12	2.132	18	5	1	$\bar{1}$	1.412	2	1.413	<1

$Ba_{0.7}As_2Ti_{4.8}V_{6.6}Fe_{2.6}O_{26}(OH)_2$ for barian tomichite. The main compositional change accompanying increasing Ba content is evidently replacement of tetravalent Ti by trivalent (Fe + V). The valence-sum calculations show that this takes place predominantly in site M(2) in the V_3O_5-type columns. There is very little difference in the occupation of the independent M(3) and M(4) components in the α-PbO_2 chains, although the lower temperature factor for M(3) suggests that this site may be enriched in Fe. (V scattering curves were used for all sites in the refinement.)

In Table 9, the calculated powder patterns for tomichite and barian tomichite are compared.

Acknowledgments

We thank Dr. E. H. Nickel for the sample of tomichite and for his helpful comments on improving the manuscript.

References

Åsbrink, Stig, Friberg, Stig, Magnéli, Arne, and Andersson, Georg. (1959) Note on the crystal structure of trivanadium pentoxide. Acta Chemica Scandinavica, 13, 603.

Ghose, Subrata, Boving, Paul, LaChapelle, W.A., and Wan, Che'ng. (1977) Reinerite, $Zn_3(AsO_3)_2$: An arsenite with a novel type of Zn-tetrahedral double chain. American Mineralogist, 62, 1129–1134.

International tables for X-ray crystallography (1974) Vol. IV. Kynoch Press, Birmingham.

Kjekshus, Arne, Rakke, Trond, and Andresen, A.F. (1974) Compounds with the marcasite type crystal structure. IX. Structural data for $FeAs_2$, $FeSe_2$, $NiAs_2$ and $CuSe_2$. Acta Chemica Scandinavica Series A, 28, 996–1000.

Mellini, Marcello, Orlandi, Paolo, and Perchiazzi, Natale. (1983) Derbylite from Buca Della Vena Mine, Apuan Alps, Italy. Canadian Mineralogist, 21, 513–516.

Moore, P.B., and Araki, Takaharu. (1976) Derbylite, $Fe^{3+}_4Ti^{4+}_3Sb^{3+}O_{13}(OH)$, a novel close-packed oxide structure. Neues Jahrbuch für Mineralogie Abhandlungen, 126, 292–303.

Nickel, E.H. (1977) Mineralogy of the "green leader" gold ore at Kalgoorlie, Western Australia. Australasian Institute of Mining and Metallurgy Proceedings, 263, 9–13.

Nickel, E.H., and Grey, I.E. (1979) Tomichite, a new oxide mineral from Western Australia. Mineralogical Magazine, 43, 469–471.

Sheldrick, G.M. (1976) SHELX-76: A programme for crystal structure determination. University of Cambridge.

Tillmans, Ekkehart, Hofmeister, Wolfgang, and Baur, W.H. (1985) Variations on the theme of closest packing: The structural chemistry of titanate compounds. Journal of Solid State Chemistry, 58, 14–28.

Zachariasen, W.H. (1978) Bond lengths in oxygen and halogen compounds of *d* and *f* elements. Journal of the Less-Common Metals, 62, 1–7.

Zaslavskiy, A.I., and Tolkachev, S.S. (1952) Structure of the α-modification of lead dioxide (in Russian). Zhurnal Fizicheskoi Khimii, 26, 743–752.

Manuscript received November 7, 1985
Manuscript accepted September 2, 1986